THE ASTROPHYSICAL JOURNAL, 236: 779–797, 1980 March 15

THE GAS DISTRIBUTION IN THE CENTRAL REGION OF THE GALAXY. III. A BARLIKE MODEL OF THE INNER-GALAXY GAS BASED ON IMPROVED H I DATA

H. S. LISZT
National Radio Astronomy Observatory,[1] Green Bank, West Virginia
AND
W. B. BURTON
Department of Astronomy, University of Minnesota
Received 1979 June 13; accepted 1979 September 17

ABSTRACT

We discuss the morphology and kinematics of gas lying within 2 kpc of the galactic nucleus in terms of material confined to a barlike structure which is tilted 24° with respect to the rotation axis of the Galaxy at large. The model embodies only motions along closed elliptical paths and thereby involves no net flow of mass out of the inner regions of the Galaxy. Angular momentum is conserved because the motions obey the equal-areas law. As with the circular model employed earlier in this series of papers, the tilted-bar model accounts for the appearance of a diverse assortment of individual condensations in position-velocity maps, such as the nuclear disk, the connecting arm, the molecular ring, and other discrete features usually considered to have been ejected from the core of the Galaxy. The model accounts for these features without any local kinematic perturbations or density enhancements.

Subject headings: galaxies: nuclei — galaxies: Milky Way — galaxies: structure — radio sources: 21 cm radiation

I. INTRODUCTION

The structure of the central region of our Galaxy is usually characterized as a patchwork of kinematically and morphologically diverse features representing a wide variety of physical phenomena (see the review by Oort 1977). Interpretations include descriptions of many apparently individually ejected H I features (e.g., van der Kruit 1970; Cohen and Davies 1976) and of an apparently expanding molecular ring massing some $10^8\ M_\odot$ in the galactic equator (e.g., Scoville 1972; Kaifu, Kato, and Iguchi 1972). For a few features, in particular the 3 kpc arm, alternatives to the nuclear-ejection interpretations have been offered which involve motions in dispersion orbits (Shane 1972; Simonson and Mader 1973) or along closed elliptical streamlines lying in the galactic equator (Peters 1975). In the absence of any apparent reason for relating gas observed at widely separated positions and velocities, interpretations of the various galactic-core phenomena have necessarily concentrated more on deriving parameters of individual features than on finding unifying underlying structures or a framework which might serve as a guide to a satisfactory physical interpretation of the region as a whole.

Explanations in terms of separate ejecta are unsatisfying because of the large number of unrelated events specified, and because of the unknown nature of the ejection mechanism and the required collimation of this mechanism. Also worrisome in the context of ejection interpretations is the observed strict confinement of H I emission to velocities $|v| \lesssim 280$ km s^{-1} (Burton, Gallagher, and McGrath 1977), although initial speeds of about 750 km s^{-1} are necessary for ejected material to overcome the galactic gravitational potential sufficiently to reach the observed z-distances (Oort 1977). The proposed expanding molecular ring and pure-rotation nuclear disk offer special difficulties in the context of the ejection hypothesis. Thus it is difficult to understand how the quiescent conditions suitable for efficient formation of molecules can prevail in the presence of violent activity, just as it is difficult to understand how an expanding ring could be within the nuclear disk which itself contains matter which is totally dynamically relaxed and in purely circular orbits. Regarding the relaxed nature of the proposed nuclear disk, it is bothersome that the observed feature resembles a *half* disk, with the sharp border of this half disk occurring at the observer-specific direction $l = 0°$.

The dispersion orbit and elliptical streamline hypotheses have not been pursued as vigorously as the ejection interpretations. Earlier nonejective explanations have not been applied to features lying in the permitted velocity regime, to apparently non-continuous features isolated in position-velocity space, or in general to the many features observed away from the galactic equator (Peters 1975 considered the behavior of some features not lying exactly at $b = 0°$, such as the "135 km s^{-1} expanding arm," but only in the context of a stylized description in which the kinematics of all features were projected

[1] Operated by Associated Universities, Inc., under contract with the National Science Foundation.

onto the galactic equator). In addition, the features which have been subject to these alternative approaches have each required independent specification of the relevant kinematic parameters.

Although the existence of a single structure coherent over the entire inner region of the Galaxy is not usually assumed, it would simplify the required interpretation if such a structure could satisfy discrepant aspects of the data. In Papers I and II of this series (Burton and Liszt 1978 [Paper I]; Liszt and Burton 1978 [Paper II], we suggested a unifying underlying structure which accounts for many features located within 2 kpc of the galactic nucleus. Essentially all of the inner Galaxy gas is located in a distribution which is tilted some 25° with respect to the rotation axis of the Galaxy at large (appearing at a position angle of 22° with respect to the galactic equator), and essentially all of the inner Galaxy gas shares a pervasive component of noncircular motion. If the complete gas distribution is viewed as tilted, and if the consequences of velocity crowding are accounted for, many of the apparently discrete features both in the optically thick CO spectra and in the optically thin H I spectra can be explained. In these terms, we were able to show by comparison of simulated H I and CO profiles with observations that a single large-scale and slowly varying velocity field could alone (even in the presence of gas at constant density) give the appearance of containing a diverse assortment of individual condensations.

The interpretation given in Papers I and II depends crucially on three underlying principles: (i) the importance of the velocity-crowding parameter $|dv/dr|$ (which determines the opacity at a given line-of-sight velocity) to the radiative transfer, (ii) the confinement of the core gas to a tilted distribution, and (iii) the pervasive character of the noncircular kinematics. The first two of these three principles are easy to defend; defense of the third is more difficult because of the alternative interpretations possible. This paper concerns itself with the nature of the noncircular motions, and offers an interpretation which we believe more plausible than the one given in Papers I and II.

i) *Regarding the kinematic parameter* $|dv/dr|$: This parameter dominates the appearance of spectra whenever the gas distribution is more or less widespread and the line-of-sight velocity field is not completely trivial. This situation occurs in general in the galactic plane (see Burton 1971) and certainly pertains to the inner Galaxy.

ii) *Regarding the confinement of most of the core gas to a tilted distribution:* A number of earlier investigations have indicated structures inclined to the galactic plane. Thus in 1967 Kerr showed that H I emission at the extreme permitted velocities originates preferentially from the opposed quadrants $l > 0°$, $b < 0°$ and $l < 0°$, $b > 0°$. Kerr and Sinclair (1966) showed that a ridge line in the 20 cm radio continuum flux is inclined in the same sense. It was noted by van der Kruit (1970) and discussed in some detail by Cohen (1975) and Cohen and Davies (1976) that the apparently isolated H I features at forbidden velocities also occur preferentially in these two opposed quadrants. This was taken as evidence of a favored collimation axis for the nuclear activity. At the recent IAU Symposium 84 on "The Large Scale Characteristic of the Galaxy" several papers (by Cohen (1979), by Sinhah (1979*a*) by us, and by others), and numerous discussion remarks included in the proceedings of the symposium focused attention on the tilted nature of the nuclear H I emission. In our own work reported in Paper I we showed that the tilted distribution encompassed essentially all of the gas, whether at forbidden or permitted velocities, within 2 kpc of the nucleus. In Paper II we showed that the molecular gas, traced by observations of the 2.6 mm line of CO, also partakes in the systematic deviations from the $b = 0°$ equator. Finally we note that the Ne II results reported by Lacy *et al.* (1979) show that the ionized gas in the innermost (~ 1 pc) core of the nucleus appears to be rotating about an axis tilted by an even larger amount, but still oriented in the same sense as the nuclear gas at larger distances.

iii) *Regarding the pervasive noncircular kinematics:* The applicability of noncircular motions to features at permitted velocities is most convincingly shown by demonstrating that observed spectral features in the permitted regime can be accounted for by the same kinematics more directly required by the spectral features in the forbidden regime. In Papers I and II we based our interpretation on the simplest possible description of the velocity fields, involving separate and independently varying rotation and expansion motions. Although this circularly symmetric, expanding disk model can give simulated spectra in good agreement with the observed situation, the model is physically implausible on several counts: (*a*) the form of the disk is not preserved because of the expansion, (*b*) a large net flux of mass is involved, and (*c*) the ad hoc motions within the disk have no physical motivation. In this paper we discuss a model of the inner-Galaxy gas which embodies motion along closed elliptical paths (presumably streamlines). Although slightly more complex than our previous model, it does eliminate some of the principal conceptual difficulties of the original description.

Several earlier papers invoke a bar (or other nonaxisymmetric but large-scale configuration such as a high-pitch-angle spiral) to explain isolated features of the data. Most relevant in the present context are the elliptical streamline and dispersion orbit models worked out by Peters (1975), Shane (1972), and Simonson and Mader (1973) (see also Sinha 1979*b* and other papers therein). These models have a reasonable dynamical basis, require no ejective activity in the nucleus, and involve no net flux of matter out of the inner Galaxy. The dispersion-ring models were directed primarily toward the analysis of the 3 kpc arm, although Simonson and Mader did show that, with some modifications to the parameters, their model can also reproduce the H I feature which crosses $l = 0°$ at 70 km s^{-1}. Peters's elliptical streamline model reproduced several of the high-velocity

features near the galactic equator. Peters could not exclude, however, the existence of large expansion motions for some of the observed features, nor did he address the numerous features lying well above and below the equator. In this paper, we incorporate elliptical streamline kinematics into the tilted disk description, and, analyzing the radiative transfer consequences of the model in the same way as in Papers I and II, show that many of the apparent spectral peculiarities are accounted for.

II. NEW H I OBSERVATIONS

New observations of the inner-Galaxy H I were made in 1978 August, October, and November at the 140 foot (43 m) telescope in Green Bank. The observing procedures for the new data were the same as those described in Paper I, so that the new and existing material could be combined to yield a completed H I survey with 0°.5 beam spacings in both longitude and latitude over the region $349°.0 \leq l \leq 13°.0$, $|b| \leq 10°.0$ (excluding $|b| = 9°.5$). The integration time per profile was 600 seconds for the grid points within a band about 6° wide in latitude centered on the line $b = -l$ tan 22°; outside this band the integration time was at least 300 seconds. The velocity resolution of the data is 2.75 km s^{-1}, although the spectra used here have been digitally smoothed to a resolution of 11 km s^{-1}. The typical rms noise level of an unsmoothed spectrum is 0.06 K. In this paper, the intensities are given in terms of the measured antenna temperatures; the radial velocities are referred to the local standard of rest defined by the standard solar motion of 20 km s^{-1} toward $\alpha, \delta = 18^h, +30°$ (epoch 1900.0). The full survey contains observations at 1845 positions; it will be given a taxonomic discussion in a separate paper.

III. GEOMETRY AND KINEMATICS OF THE TILTED ELLIPTICAL-DISK MODEL

The gas motions are constrained to lie in planes parallel to the disk midplane which is specified by the doubly primed axes, x'' and y'', illustrated in Figure 1. The position angle α involves a counterclockwise rotation in the plane of the sky; i is the conventionally defined inclination angle. In order to specify the orientation of the elliptical streamlines, it is necessary to introduce the additional angle θ_0 shown also in Figure 1. For $i = 90°$, $\alpha = 0°$, and $\theta_0 = 0°$, the minor axes of the streamlines located in the midplane of the model lie on the Sun-center line. Because the parameters α, i, and θ_0 are strict constants, there is no warping of the model. The only parameter which varies with distance from the midplane $z_d = 0$ pc is the gas volume density $n(z_d) = n(0) \exp[-0.5(z_d/h_d)^2]$, where $n(0) = 0.33$ H I atoms cm^{-3} and $h_d = 0.1$ kpc as in Paper I.

In the circularly symmetric model, description of the kinematics involved specification of two free and independently varied orthogonal functions representing rotation and expansion within the tilted disk. In the present case, the motions are more strongly

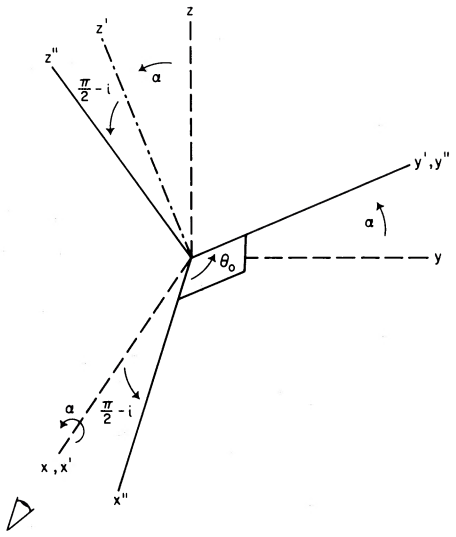

FIG. 1.—The coordinate transformations used to specify the orientation of the model. The angle α represents a counterclockwise rotation about the Sun-center line to form the primed coordinate system. This is followed by a similar rotation of $\pi/2 - i$ about the y' axis to form the doubly-primed coordinates. The angle θ_0, measured from the x'' axis, specifies the orientation of the semiminor axes of the elliptical streamlines.

coupled to the geometry of the model. They are specified as follows. We parametrize the figures of the streamlines in terms of their semiminor axes b_d; b_d may vary between 0 and a maximum value b_d'. The variation of ellipticity is then contained in a function $a_d(b_d)$, where a_d is the semimajor axis. We assume that motion along the streamlines follows the equal-areas law, conserving specific angular momentum, so that all remaining kinematic aspects of the model are contained in a single function $v_t(b_d)$ which describes the variation of circulation speed along the minor axes. One of the biggest differences between the circular and elliptical models is the extent to which the figure of the latter model influences the perceived kinematics. Although more effort is required to specify the present geometry, only a single function, $v_t(b_d)$, is explicitly kinematical in nature.

As in the earlier work, the model parameters have been determined by an iterative comparison of observed and simulated data. The simulated spectra were generated in the manner described in Paper I, but, because the ellipticity varies, it was necessary to solve iteratively the equation of an ellipse at each point intersecting the model. Once this was done and the appropriate value of b_d was known, motions along the relevant path could be decomposed into the radial and circular components; then equation (5) of Paper I yielded directly the perceived radial velocity. In Papers I and II the bulk of the model-fitting involved material near the locus $b = -l$ tan 22° which was found from moment maps and other displays of the data to be the apparent axis of kinematic symmetry. This indicated the position angle value $\alpha = 22°$

directly. Similar considerations might be thought to constrain the geometry of the present model such that the long axes of the streamlines would be aligned near a position angle 22°. This may be represented in the form

$$\cos i = \tan (22° - \alpha)/\tan \theta_0 ,$$

which shows that the true position angle $\alpha < 22°$ if $\theta_0 > 0°$. In practice, models which were constrained in this manner did not fit the data as well as those in which the apparent position angle of the long axes was allowed to be somewhat larger. This situation arises because of the large values $\theta_0 \approx 40°$ required of the models. The apparent kinematic symmetry axis of such models is perceived at a position angle noticeably less than the true position angle, which is not the case for a circular disk or when $\theta_0 \sim 0°$.

The geometrical parameters found for the model discussed below are:

$$i = 70° , \quad \alpha = 13\overset{\circ}{.}5 , \quad \theta_0 = 41\overset{\circ}{.}5 , \quad b_d' = 0.60 \text{ kpc}$$

$$a_d/b_d = 1.6 + 1.5\, b_d/b_d' .$$

A projection of this model onto the plane of the sky is shown in Figure 2. The axes of the tilted planes containing the streamlines make an angle $\cos^{-1}(\sin i \cos \alpha) = 23\overset{\circ}{.}7$ with respect to the rotation axis

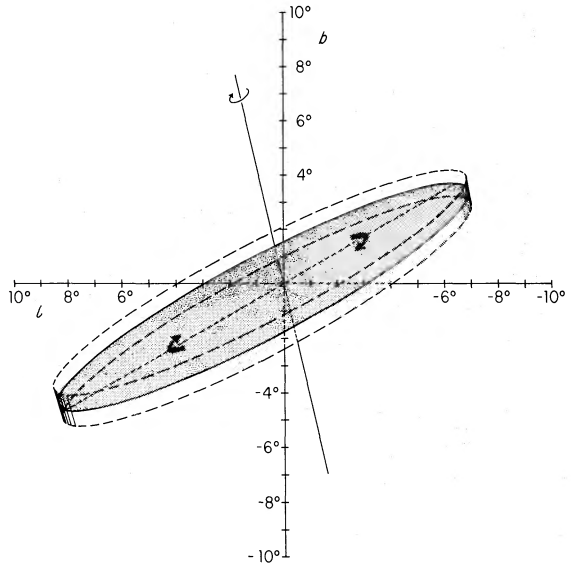

FIG. 2.—Appearance of the model tilted gas distribution as projected onto the plane of the sky in the angular coordinates of the observations. The shaded solid-line approximate ellipse represents the equatorial plane $z_d = 0$ kpc of an elliptical cylinder with semiminor axis $b_d = 0.60$ kpc and semimajor axis $a_d = 3.1 b_d$; the dashed lines are drawn at heights $z_d = \pm 0.10$ kpc. The orientation of the model is given by $\alpha = 13\overset{\circ}{.}5$, $i = 70°$, $\theta_0 = 41\overset{\circ}{.}5$. The true semimajor axis of the midplane of the model, drawn as a dashed line, appears at position angle 29°; note that because of projection effects this position angle characterizes neither the axis of apparent kinematic symmetry ($\alpha = 22°$) nor the position angle of the inclined plane in which it lies ($\alpha = 13\overset{\circ}{.}5$).

of the Galaxy at large, which is almost identical to the corresponding value of $24\overset{\circ}{.}9$ obtained for the circular disk. However, the values of $90° - i$, here 20°, and α, $13\overset{\circ}{.}5$, have approximately interchanged their values compared to the earlier work (in which $\alpha = 22°$, $90° - i = 12°$). Because of the large value of θ_0 indicated, the outermost ellipse extends to 1.9 kpc from the galactic center; this distance is larger than the 1.5 kpc radius of the circular disk. The streamlines become more circular in the inner regions of the model to take advantage of the relatively large line-of-sight projection of the rotational velocity component and relatively small projection of the radial velocity component near the subcentral point. Models in which the ellipticity is constant or increases inward fit badly both the permitted and forbidden velocity patterns.

The functional form of the rotation speed $v_t(b_d)$ at the minor axes is

$$v_t(b_d) = 360 \text{ km s}^{-1} [1 - \exp (-b_d/0.100 \text{ kpc})] .$$

Superposed on the flow at all positions is a velocity dispersion $\sigma = 9$ km s^{-1}, as in Papers I and II. A speed of 360 km s^{-1} is certainly higher than that obtained from analysis of the inner-Galaxy material in terms of pure rotation (cf. Oort 1977) and is also higher than the greatest speed ($\sim$250 km s^{-1}) obtained in the circular model of Paper I. This difference stems from the need to produce outward velocity projections of order 150 km s^{-1} in a situation where only a fraction of the orbital velocities is in the radial direction and where this fraction is largest away from the minor axis when the circulation is itself slower. The addition of azimuthal forces would lower the required maximum circulation speed, but there is at present no treatment of the inner-Galaxy dynamics which would serve as a guide in their specification.

The model described here does not incorporate a pattern speed or solid-body rotation of the elliptical figures about their own polar axis. Although it is likely that more complicated models could be formulated to include such effects, the ability of the present disk to reproduce the observations is impaired unless the superposed pattern speed is less than 10 km s^{-1} kpc^{-1}. In the present context it is not clear that the addition of another adjustable parameter such as the pattern speed would enhance the plausibility of the kinematic modeling process.

We remind the reader that a number density varying only with z_d has been employed here so as to emphasize the importance of projection effects in illustration of the kinematic patterns resulting from the model. For a true steady state the gas density would be required to satisfy the equation of continuity, which permits a constant density if and only if the divergence of the gas flow vanishes. With motion following the equal-areas law, this condition on the flow is equivalent to demanding constant ellipticity for all the streamlines, in which case the continuity equation is satisfied for any density distribution of the form $n \propto b_d^{-q}$, with $q \geq 0$. Solution of the continuity equation for arbitrary variation of ellipticity (as required here) is

difficult and would, in any case, not change the regions of position-velocity space occupied by the model profiles. Within these regions one would expect changes in the detailed shapes of the model profiles, particularly at low latitudes where the line of sight traverses longer paths through the model. Undoubtedly, some new "features" representing actual density variations would be created; these would however, lie within the regions indicated in the diagrams below.

IV. MORPHOLOGY OF THE TILTED INNER-GALAXY GAS DISTRIBUTION

a) The Tilt of the Inner-Galaxy Gas Revealed by Moment Maps

In Figure 3 we show spatial maps of H I column densities found by integrating the emission over the indicated velocity ranges. The maps in Figure 3*a* were constructed using material at $v > 200$ km s^{-1} in the quadrant $l < 0°$, and at $v < -200$ km s^{-1} in the quadrant $l < 0°$. The contours representing this so-called permitted-velocity material show a marked and quite coherent departure from $b = 0°$ on both sides of the plane $l = 0°$. That the data are skewed with respect to their overall symmetry axis indicates that material moving with noncircular motions is contributing significantly even though this material occurs at velocities which are not "forbidden" in the usual sense. Figures 3*b* and 3*c* show the integrated emission at velocities $|v| < 200$ km s^{-1} and indicate a substantial distribution of emission with obviously noncircular motions. The emission patterns in both of these figures cross the plane $l = 0°$ rather smoothly, although the appearance of the positive-velocity data

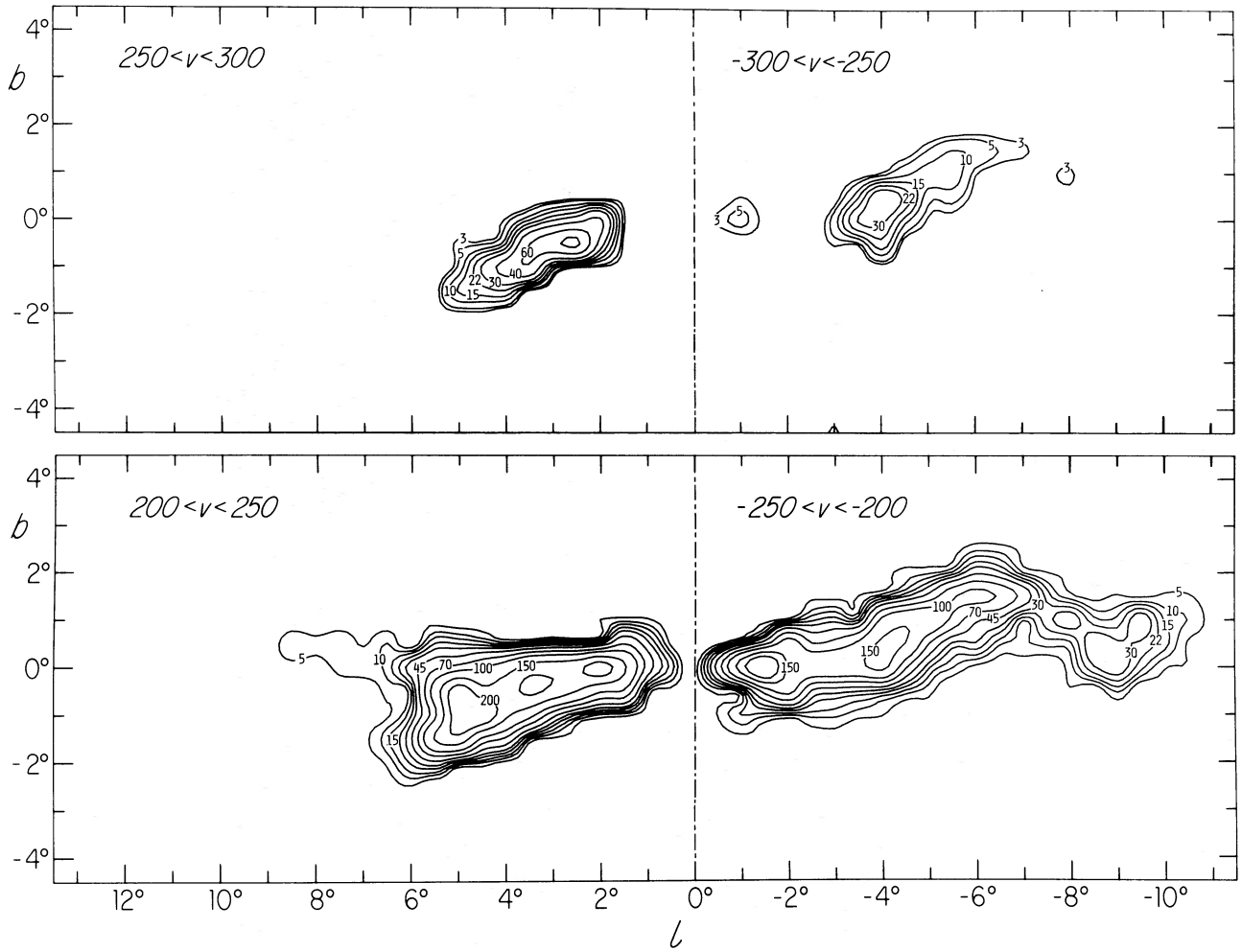

FIG. 3.—Maps or the plane of the sky of observed H I antenna temperature integrated over selected velocity ranges. The contours are labeled in units of K km s^{-1}. At a distance 10 kpc, a contour level 100 K km s^{-1} over a solid angle of one square degree corresponds to $7 \times 10^4\ M_\odot$ if, as seems likely, the gas is optically thin. The maps display separately emission from material occurring at velocities which are forbidden and permitted in the sense of circular galactic orbits. Irrespective of the forbidden or permitted nature of the velocities, the integrated emission departs coherently from $b = 0°$ on both sides of the plane $l = 0°$.

FIG. 3*a*.—Contours of observed antenna temperature integrated over the highest observed velocities which are permitted in the sense of circular galactic rotation.

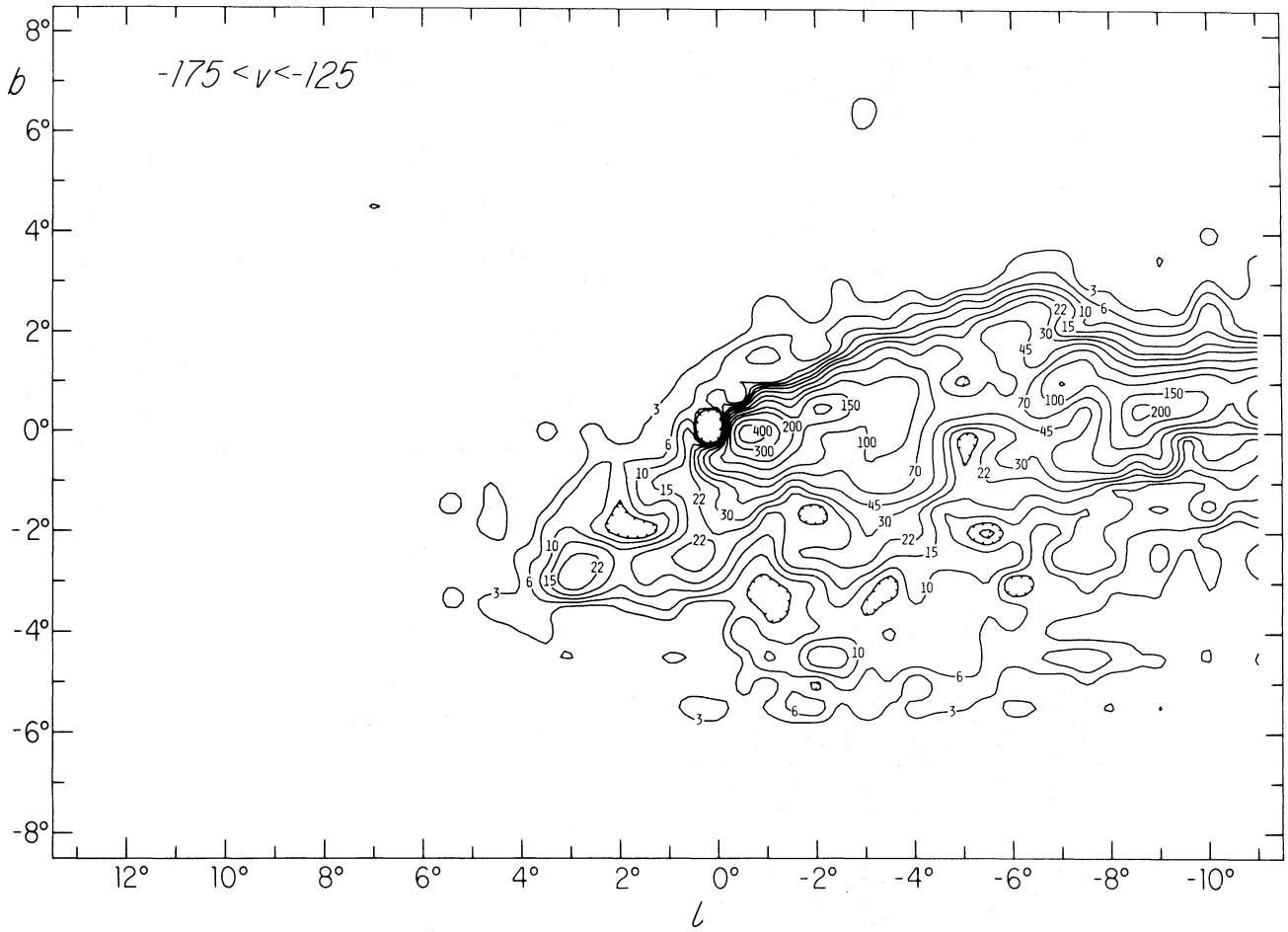

FIG. 3*b*.—Contours of observed antenna temperature integrated over the velocity range $-175 < v < -125$ km s^{-1}. For $l > 0°$, emission in this velocity range is forbidden in terms of circular galactic motions.

is influenced by the presence of the "+135 km s^{-1} expanding arm" at $b = 0°.5$, $l \lesssim -2°$.

The observed moment maps show the general characteristic of having positive-velocity gas lying above (and negative-velocity gas below) $b = 0°$ at $l = 0°$. This follows because $i < 90°$ and because the relevant velocities are contributed predominantly by the noncircular component of motion. Moment maps generated using the elliptical streamline synthetic spectra show the same characteristic. The upper panels of Figure 4 contain the model moment maps for the range $125 \leq |v| \leq 175$ km s^{-1}. Because the velocity range used to construct them is limited, and because they are free of contamination of emission from the remainder of the Galaxy, these model maps each have the appearance of comprising two separately collimated but nonaligned jets originating 1° away from Sgr A. This nonalignment with $l = 0°$, $b = 0°$ is seen clearly in the positive velocity emission at $b \sim 2°$–$4°$, $-4° \leq l \leq 0°$, which comprises feature J2 of Cohen (1975) and Cohen and Davies (1976) as well as emission discussed by Sanders and Wrixon (1972*b*). Although this combined emission is usually considered to be a prototypical example of gas which has been ejected from the vicinity of Sgr A, its peculiar disposition would seem to require additional assumptions in such a picture.

Figures 3*d* and 3*e* show the complete distribution of H I integrated intensities over the velocity ranges $100 \leq |v| \leq 300$ km s^{-1}. (These figures may be compared with Figures 2 and 3 in Paper I to gauge the increased sensitivity and coverage afforded by the newer data.) The tilted nature of the forbidden-velocity gas persists to $|l| = 5°$ or 6°. Comparable model moment maps are shown in the lower panels of Figure 4. With the wider velocity interval, they appear more uniform than the maps in the upper panels. The modeled moment distributions show the same general general trends as are observed, including the tilted nature and extent of the moment distributions, and the zero-longitude crossings at $b \neq 0°$.

b) The Apparent Axis of Kinematic Symmetry

As was discussed in some detail in Paper I, the fundamental kinematic and spatial symmetries which are noticeably lacking in (l, v)-diagrams made at

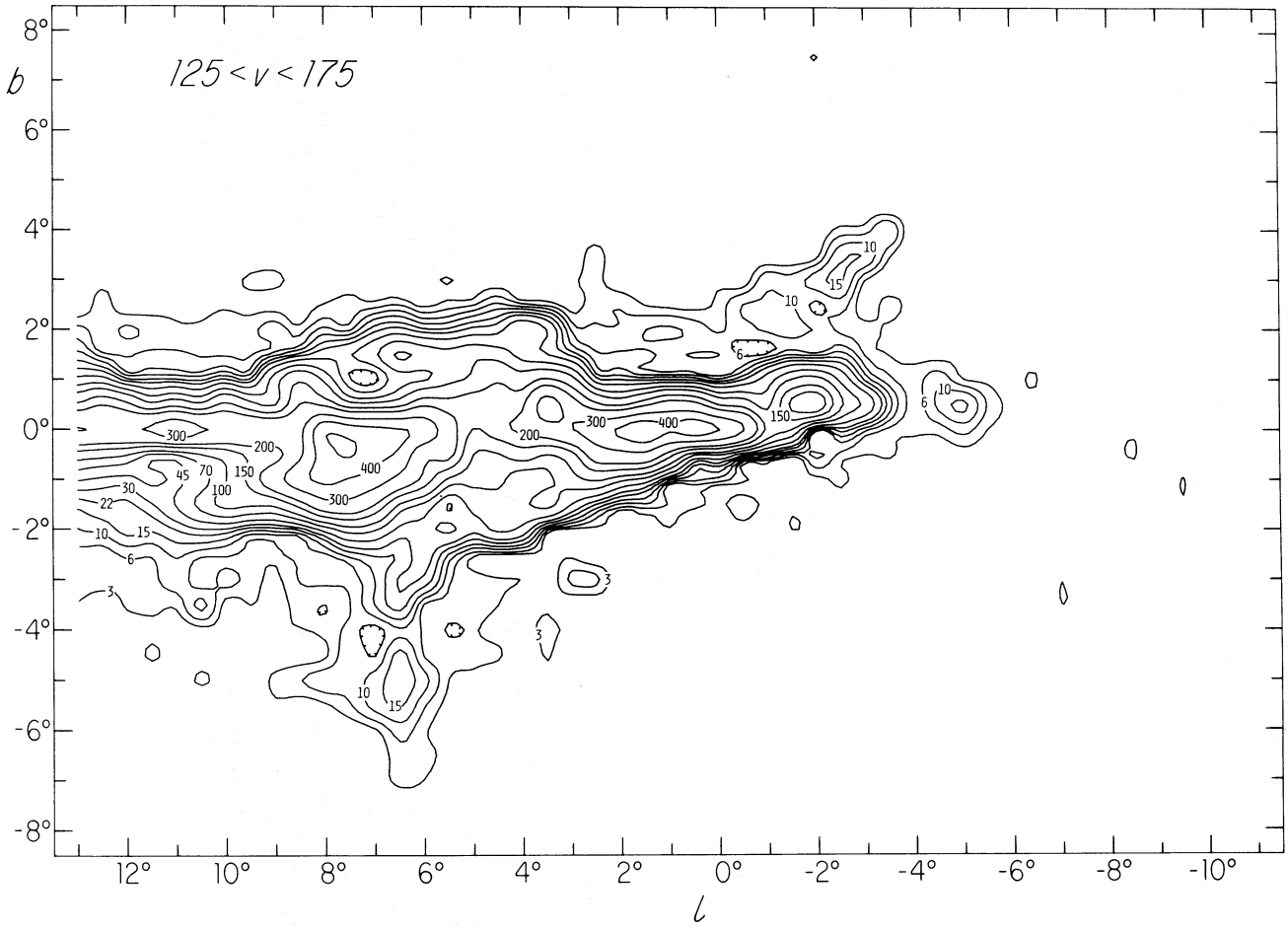

FIG. 3*c*.—Contours of observed antenna temperature integrated over the velocity range $125 < v < 175$ km s^{-1}. For $l < 0°$, emission in this velocity range is forbidden in terms of circular galactic motions. The emission at $b \geq 2°$, $l < 0°$ is contributed by Cohen's (1975) feature J2 and by a feature discussed by Sanders and Wrixon (1972*b*); note that this emission is clearly not aligned with $l = 0°$, $b = 0°$. At $b = 0°.5$, emission from the "135 km s^{-1} expanding arm" is present at $l = -5°$, $-2°$, $4°$, $9°$.

$b = 0°$ can be brought out by mapping along inclined loci which extend above and below the galactic equator. Such a position-velocity map, constructed at a position angle $+22°$ ($b = -l \tan 22°$) by two-point interpolation in latitude within the observed grid, is shown in Figure 5*a*. (The spectrum at $l = 0°$, $b = 0°$, was not used in order to avoid confusion due to the very strong absorption present at that position.) Figure 5*b* shows the comparable modeled situation. Obviously transgalactic hydrogen is not included. The envelopes of the terminal velocities extend continuously across the plane $l = 0°$ at both positive and negative velocities. This suggests rather directly that noncircular motions do indeed occur within the "nuclear disk" feature, and suggests consequently that the conventionally derived inner-Galaxy rotation curve based on this feature and the assumption of purely circular motion will rise more sharply and imply a greater nuclear mass concentration than justified by the present interpretation.

There are two noticeable asymmetries in the Figure 5*a* observations, only one of which is inherent in the elliptical disk model and probably a property of the inner-Galaxy gas distribution. The first of these concerns the characteristic that the emission at "permitted" positive velocities extends to larger $|v|$ than does the emission at "permitted" negative velocities. This asymmetry of the entire pattern is in the same sense and of the same magnitude as that observed between the two branches of the "expanding molecular ring" (see Paper II). In fact, all of the observed patterns reported and discussed here are somewhat displaced to positive velocities. Because the band of emission from the transgalactic gas shares in the displacement, it seems likely that the observed pervasive asymmetry is not a property specific to the inner Galaxy. Thus the 15 K contours in Figure 5*a* are centered near $v = +10$ km s^{-1} at $l = 0°$. The centroid of the velocity-longitude distributions shown for various latitudes in Figure 6 are systematically displaced over the entire range of longitude $-11° \leq l \leq 13°$. This displacement has been discussed by

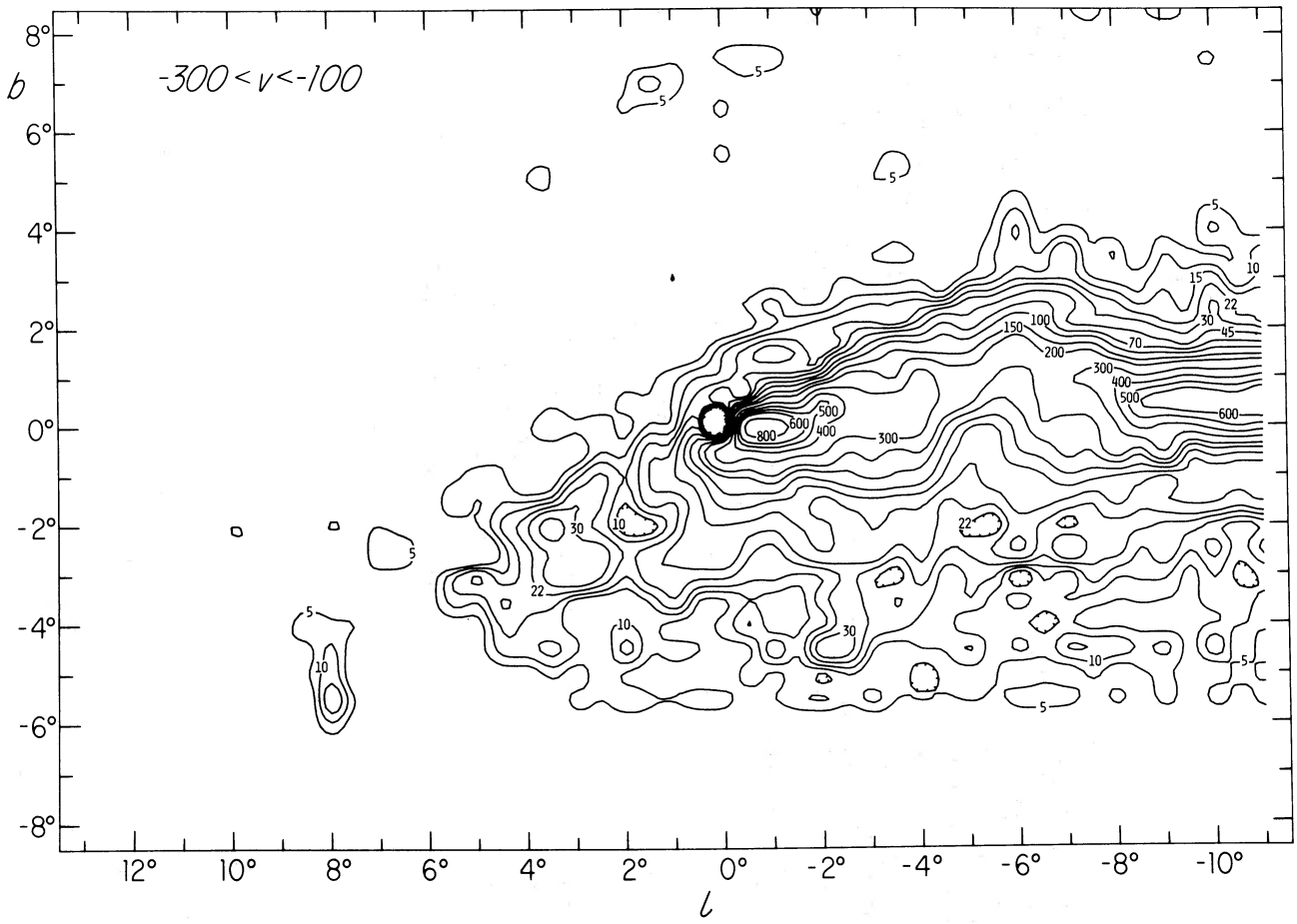

FIG. 3*d*.—Contours of observed antenna temperature integrated over the velocity range $-300 < v < -100$ km s^{-1}. The forbidden-velocity material is seen out to $l \sim 6°$.

several authors, principally by Kerr (1962) and Braes (1963), who interpreted it in terms of a motion of the solar neighborhood outward with respect to the nucleus. Whatever its cause, such a motion is sufficient to account for much of the displacement observed in the gas represented in Figure 5*a*. The second asymmetry is a property of the envelope of terminal velocities reflected in both the observed and simulated spectra shown in Figure 5. This envelope decays much more abruptly toward zero velocity at negative longitudes than at positive longitudes; in addition, emission at positive longitudes and velocities extends further in l than the corresponding emission at negative longitudes and velocities. This asymmetry occurs because the positive longitude portions of the disk are substantially nearer to the Sun and so appear larger. The maximum extent of the major axes of the modeled elliptical streamlines is 3.7 kpc; even after projection, this length is not small compared to the adopted Sun-center distance of 10 kpc.

Because both the beam size (0°.36) and the grid spacing (0°.5) are not small compared to typical departures from $b = 0°$ in the inner map regions, many details of the true distribution are undoubtedly unavailable; this problem is also compounded by interpolation. We estimate the uncertainty in the position angle of the kinematic symmetry axis to be approximately $\pm 2°$, but the observational map at position angle 20° is more symmetrical than that at 24°. The observational map at 20° has the property that the emission ridges which are prominent in the model diagram of Figure 5*b* are more pronounced than in the observational map at 22°.

The exact position of the axis of kinematic symmetry in the data is not as directly informative in the present case as in Paper I. The position angle of the planes containing the gas orbits is $\alpha = 13°.5$; the major axes of the elliptical streamlines themselves, however, occur at position angle 29°.

V. APPEARANCE OF THE ELLIPTICAL DISK MODEL IN (l, v) DIAGRAMS

a) *The* H I *Data*

The detailed kinematics of the inner Galaxy gas are more clearly shown in longitude-velocity diagrams

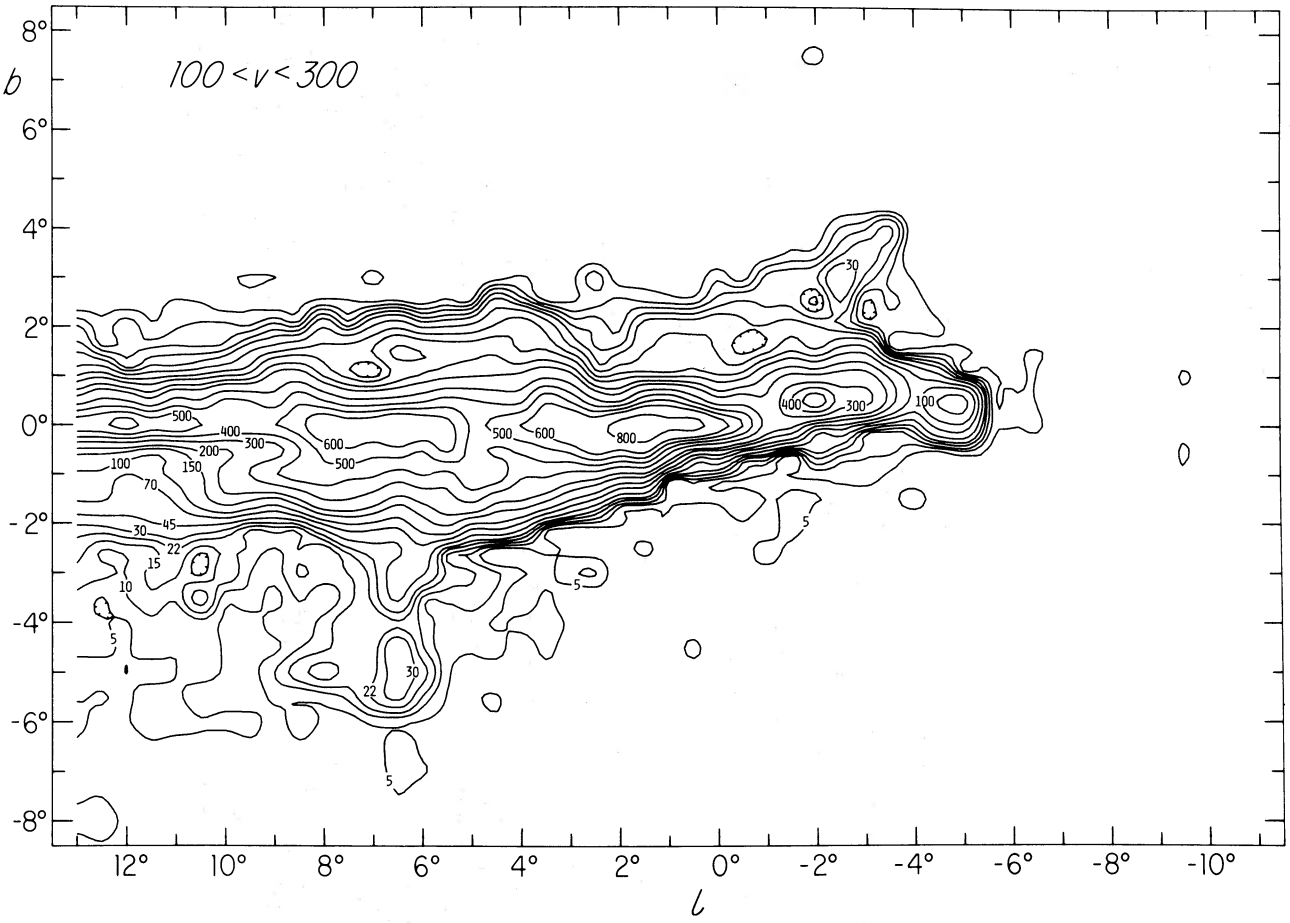

FIG. 3*e*.—Contours of observed antenna temperature integrated over the velocity range $100 < v < 300$ km s^{-1}

formed at constant latitudes than in latitude-velocity diagrams, because the signature of the inner Galaxy disk varies more slowly with position and velocity in (l, v)-diagrams and because there is generally less contamination (except at $|b| \lesssim 1°$) in these diagrams from transgalactic gas. In Paper I we showed diagrams of both types; we show here in Figure 6 a series of (l, v)-diagrams, constructed from the newer, more closely spaced, and more sensitive data. Superposed on each diagram is the pattern giving the signature of the modeled elliptical disk. In view of the extensive discussion of individual features given in Paper I and in the figure legends presented here, only a few aspects of the observations and disk signature need be noted.

i) $b = +3.^{\circ}0$ (Fig. 6*b*).—The material at $100 \lesssim v \lesssim 175$ km s^{-1}, $-3° \leq l \leq -1°$, is a combination of Cohen's feature J2 (Cohen 1975; Cohen and Davies 1976) and a pattern discussed by Sanders and Wrixon (1972*b*), Oort (1977) has taken this to be a definitive example of a feature with ejective origin.

ii) $b = +2.^{\circ}5$ (Fig. 6*c*).—The positive-velocity pattern of Figure 6*b* is weaker here; the negative-velocity emission is more pronounced. As the latitude decreases, the negative-velocity part of the disk signature moves continuously toward more positive longitudes.

iii) $b = +0.^{\circ}5$ (Fig. 6*d*).—The elliptical-disk pattern fits well within the velocity envelope of the observed gas distribution. The material at $v \sim 100$–125 km s^{-1}, $-6° \leq l \leq 0°$, is generally considered to be part of the "+135 km s^{-1} expanding arm" which is traced to $l \sim 12°$ at this latitude. An extensive discussion of this feature is given by Peters (1975), who also proposed an elliptical streamline model to account for it.

iv) $b = +0.^{\circ}5$ (Fig. 6*e*).—The negative-velocity emission pattern now clearly extends across the plane $l = 0°$. Although the elliptical-disk signature accounts well for most of this gas, which is an extension of the supposedly purely rotating nuclear disk of Rougoor and Oort (1960), it does not extend to sufficiently large positive velocities.

v) $b = -1.^{\circ}5$ (Fig. 6*f*).—As with the circular disk of Paper I, the contrary slope dv/dl of the positive-longitude emission signature is a natural consequence of kinematics employing noncircular motions; previous interpretations of this behavior invoked a central bar or high-pitched spiral arm (see Paper I).

vi) $b = -3.^{\circ}0$ (Fig. 6*h*).—A very weak feature at

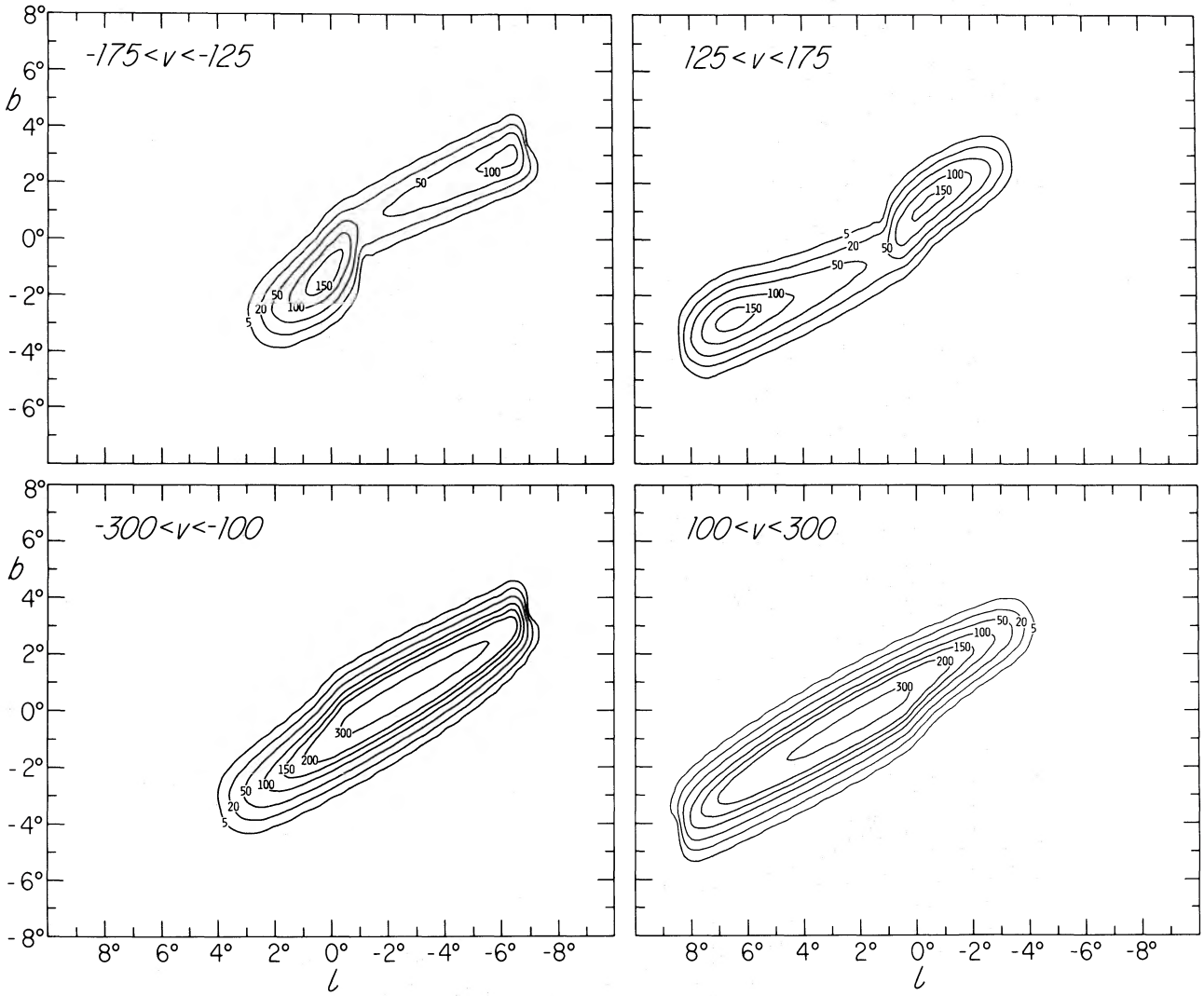

FIG. 4.—Maps of integrated H I intensity generated over the indicated velocity ranges according to the formulations of the elliptical disk model. The limited velocity interval used to construct the upper maps results in the appearance of features which could be interpreted as two separately collimated but nonaligned "jets," originating ~1° away from Sgr A. The observations, as displayed for example in Fig. 3, show analogous features.

$v \sim 70$ km s^{-1}, $-2° \leq l \leq 0°$ has not been named and is not accounted for.

vii) $b = -4.^{\circ}5$ (Fig. 6*i*).—The negative-velocity pattern encompassed by the model signature was described by Sanders, Wrixon and Penzias (1972) and by Sanders and Wrixon (1972*a*) as originating within a rotating expanding ring located 2.4 kpc distant from the galactic center. Although the elliptical disk signature provides a good fit to the positive-longitude data, one must also account in some manner for the emission pattern extending from $l \sim -8°$, $v = -175$ km s^{-1} to $l \sim 0°$, $v \sim -125$ km s^{-1}. Sanders and Wrixon (1972*a*) noted that the ring model fits to this emission are quite similar in their radii and in their velocity components (both of rotation and of expansion) to those required to fit the "+135 km s^{-1} expanding arm," and they consequently proposed the existence of a complete gaseous ring. Furthermore, because the "+135 km s^{-1} expanding arm" appears at $b = +0.^{\circ}5$ at $l > 0°$, they suggested that the ring was inclined to the galactic equator and that this inclination was the cause of the disappearance of the negative-velocity emission in this figure for $l < -8°$. The moment map in Figure 3*a* shows that this negative-velocity emission is largely confined to $b = -4.^{\circ}5$ for $l < -6°$ (and probably for $l < 0°$); similarly the "135 km s^{-1} expanding arm" is located primarily at $b = 0.^{\circ}5$ (see the peaks at $b = 0.^{\circ}5$, $l = -5°$, $-2°$, 4°, 9° in Fig. 3*c*). In any case a plane ring of radius 2.4 kpc centered on the galactic nucleus is too small for projection effects to cause it to appear simultaneously at $b = +0.^{\circ}5$ and $b = -4.^{\circ}5$ at any longitude.

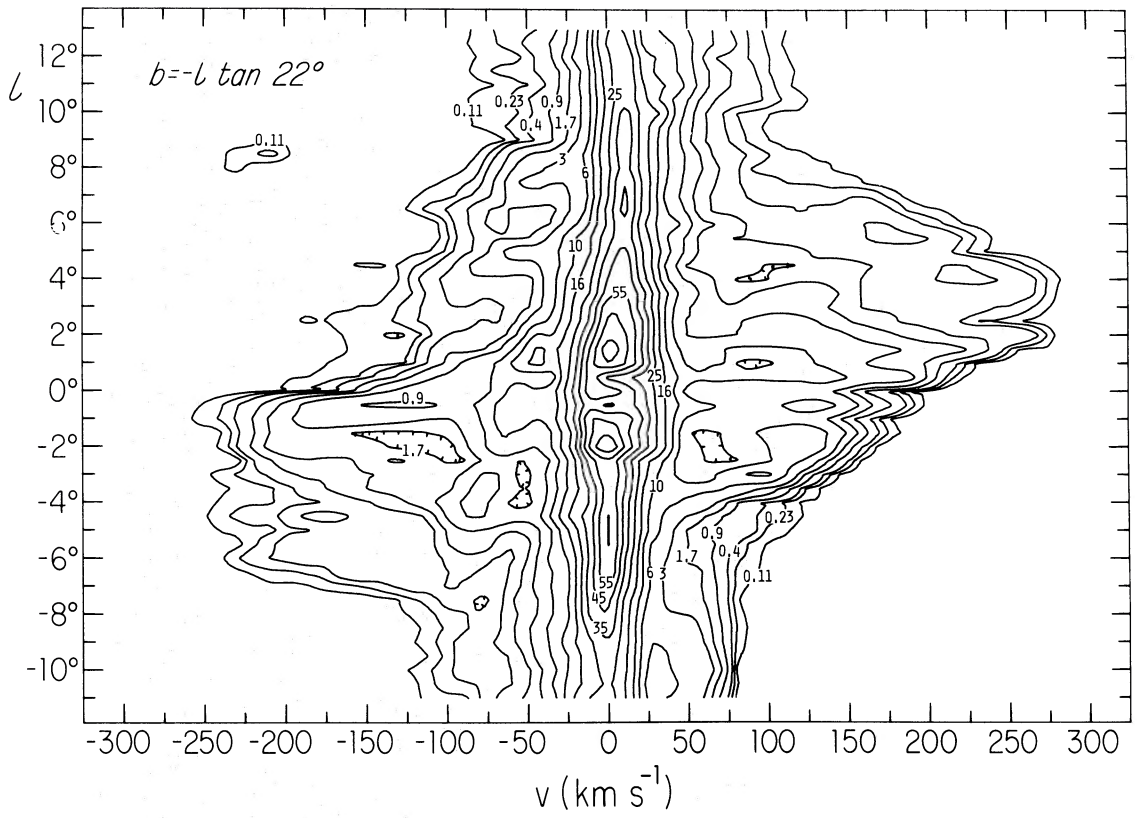

FIG. 5a

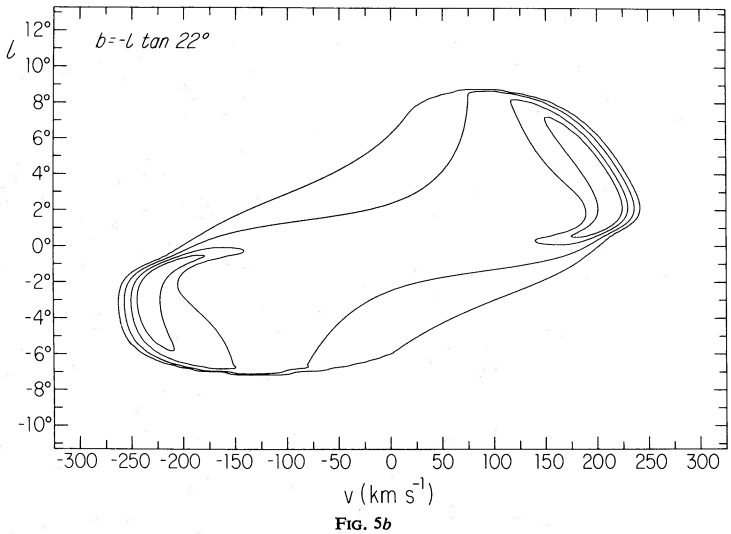

FIG. 5b

FIG. 5.—(*a*) Longitude-velocity arrangement of emission observed along the kinematic symmetry axis $b = -l \tan 22°$. This map reveals the extent of the tilted fundamental distribution of gas in the inner Galaxy and shows its kinematic and positional symmetry. In order to avoid confusion due to absorption attributable to the Sagittarius continuum sources, the spectrum at l, $b = 0°$, $0°$ was replaced by one derived by interpolation within the observed grid. (*b*) Longitude-velocity arrangement of simulated emission generated following the precepts of the inclined elliptical disk model. The simulated profiles represent only emission from the inclined inner Galaxy distribution. Thus they do not contain emission from material in the Galaxy at large; in the observed situation shown in Fig. 5*a*, such emission contributes the band of intensities centered near $v = 0$ km s^{-1}.

FIG. 6.—(*a*) Emission in the (l, v)-plane at $b = +4.^{\circ}5$. This cut intersects the inner-Galaxy tilted elliptical disk far above its mean plane and consequently shows only a weak signature from it. (*b*) Emission in the (l, v)-plane at $b = +3.^{\circ}0$. The observed positive-velocity manifestation of the disk at $l = -3°$ was discussed as a separate entity by Sanders and Wrixon (1972*b*); the disk signature at higher positive velocities near $l = -1°$ encompasses Cohen's (1975) separate feature J2.

FIG. 6.—(*c*) Emission in the (l, v)-plane at $b = +2.^{\circ}5$. The positive-velocity emission near $-1° < l < 0°$ at $v = 100$ km s^{-1} encompasses van der Kruit's (1970) feature VII and Cohen's (1975) feature J2, as well as a feature discussed by Sanders and Wrixon (1972*b*). The negative-velocity manifestation of the disk, near $l = 6°$, has not been discussed separately. (*d*) Emission in the (l, v)-plane at $b = +0.^{\circ}5$. The appearance of individual features is obscured within 1° of the galactic equator by emission from the Galaxy at large. The model successfully accounts for the observed pattern shift to negative longitudes. Our discussion does not deal with the 3 kpc arm, which crosses $v = -100$ km s^{-1} at $l = -8°$ in the maps at $b = 0°$ and $\pm 0.^{\circ}5$.

FIG. 6.—(*e*) Emission in the (l, v)-plane at $b = -0.^{\circ}5$. As is the case in the cuts at $b = 0.^{\circ}0$ and $+0.^{\circ}5$, isolated features are obscured in this cut by the contribution of emission from the Galaxy at large. The extended feature at $l > 1°$, $100 < v < 250$ km s^{-1} is Rougoor's (1964) "connecting arm." The "rotating nuclear disk" feature near $l = 0°$ is accounted for but has, of course, a very different interpretation in the terms of the model. (*f*) Emission in the (l, v)-plane at $b = -1.^{\circ}5$. The model contours encompass the following: Cohen's (1975) feature J4, in the vicinity of $l = 4°$, $v \approx 120$ km s^{-1}; van der Kruit's (1970) feature XII at $2° \leq l \leq 5°$, $v < 0$ km s^{-1}; the "connecting arm" of Rougoor (1964; cf. III*a* of Cohen 1975) at $l > 3°$, $100 \leq v \leq 250$ km s^{-1}; the minor feature V of van der Kruit and Cohen at $l = 0°$, $v = -110$ km s^{-1}; and feature E of Sanders *et al.* (1972) at $l < 0°$, $v \approx -180$ km s^{-1}.

FIG. 6.—(*g*) Emission in the (l, v)-plane at $b = -2.^{\circ}5$. The concentration of emission near $l = 6°$, $v = 160$ km s^{-1} is accounted for by the model; it is Cohen's (1975) apparently isolated feature J4. The region at negative velocities contains, within the boundaries predicted by our synthesis, feature VII of van der Kruit (1970) at $3° < l < 6°$, $v \approx -50$ km s^{-1}; feature X of van der Kruit at $3° < l < 5°$, $v \approx -120$ km s^{-1}; feature E of Sanders *et al.* (1972) at $-2° < l < 2°$, $v \approx -160$ km s^{-1}; and a feature discussed separately by Sanders *et al.* (1972) at $1° < l < 3°$, $v \approx -90$ km s^{-1}. The observational distinction among these various features is not very clear, a point also consistent with our synthesis. (*h*) Emission in the (l, v)-plane at $b = -3.^{\circ}0$. The emission concentration between $l = 5°$ and 8° at positive velocities is Cohen's (1975) feature J5; we see no way to distinguish it from his J4. Within the negative velocity boundaries predicted by our model are the same features mentioned in the caption for Fig. 6*g*.

FIG. 6.—(*i*) Emission from the (l, v)-plane at $b = -4.^{\circ}5$. Cohen's (1975) feature J5 at $l \sim 7°$, $v \sim 100$ km s^{-1} and van der Kruit's (1970) feature X at $2° < l < 5°$, $v \sim -100$ km s^{-1} are inherent in our model. The elliptical disk signature lies at negative velocities on the locus of Sanders and Wrixon's (1972*a*) suggested ring of gas 2.4 kpc distant from the galactic center. Shane's feature (Saraber and Shane 1974) at $l = 8°$, $v = -220$ km s^{-1} and the Sanders and Wrixon (1972*b*) feature (J1 of Cohen 1975) at $l = -3°$, $v = -140$ km s^{-1} are not accounted for by the model, although both lie near the fundamental plane of the tilted model. (*j*) Emission from the (l, v)-plane at $b = -5.^{\circ}5$. The disk signature at $b = -5.^{\circ}5$ is more pronounced than that at $b = +4.^{\circ}5$ because the negative-latitude, positive-longitude portion of the disk is substantially nearer the Sun. At the distance of the galactic center, the material in this figure lies almost 1 kpc below the galactic plane.

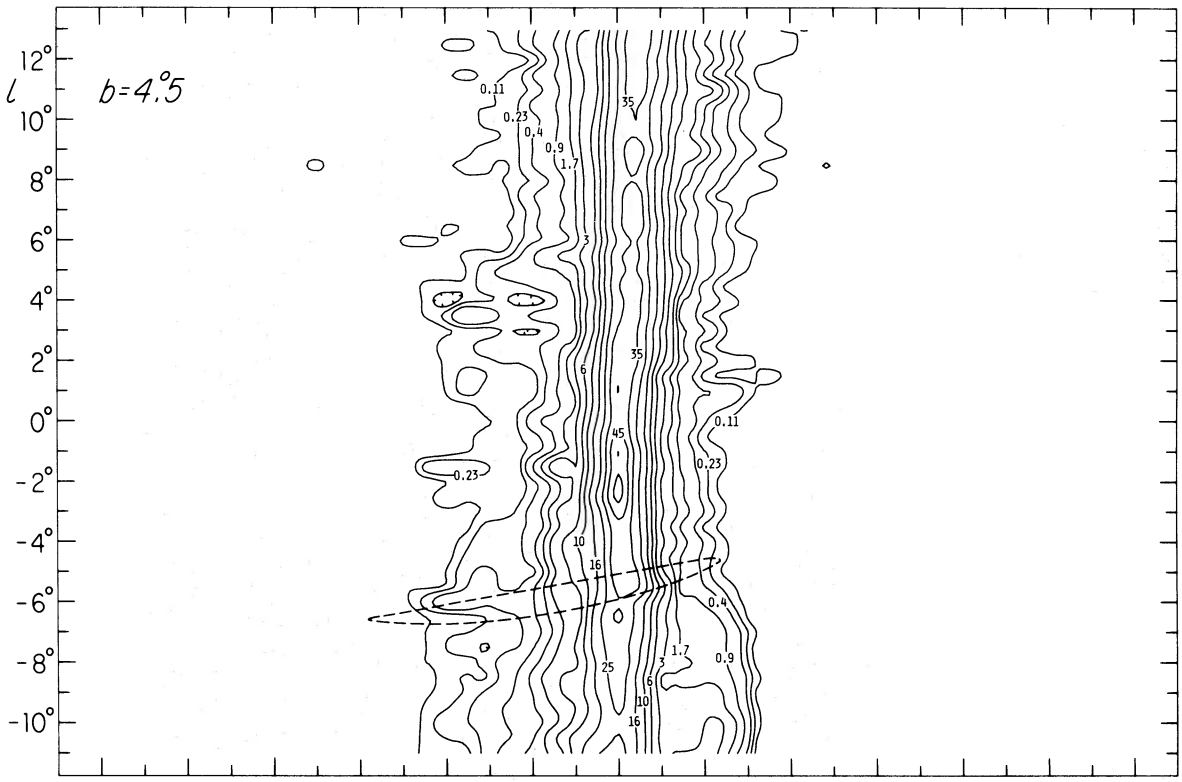

FIG. 6*a*

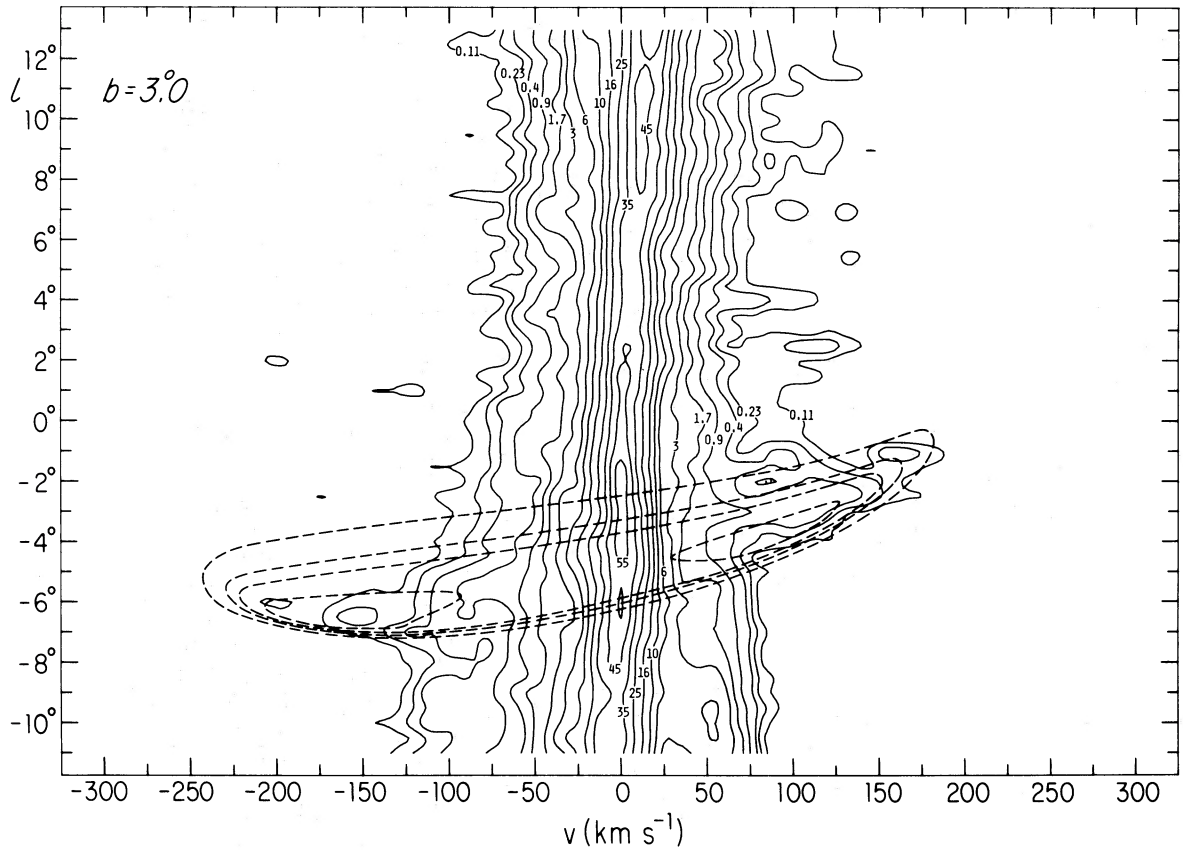

FIG. 6*b*

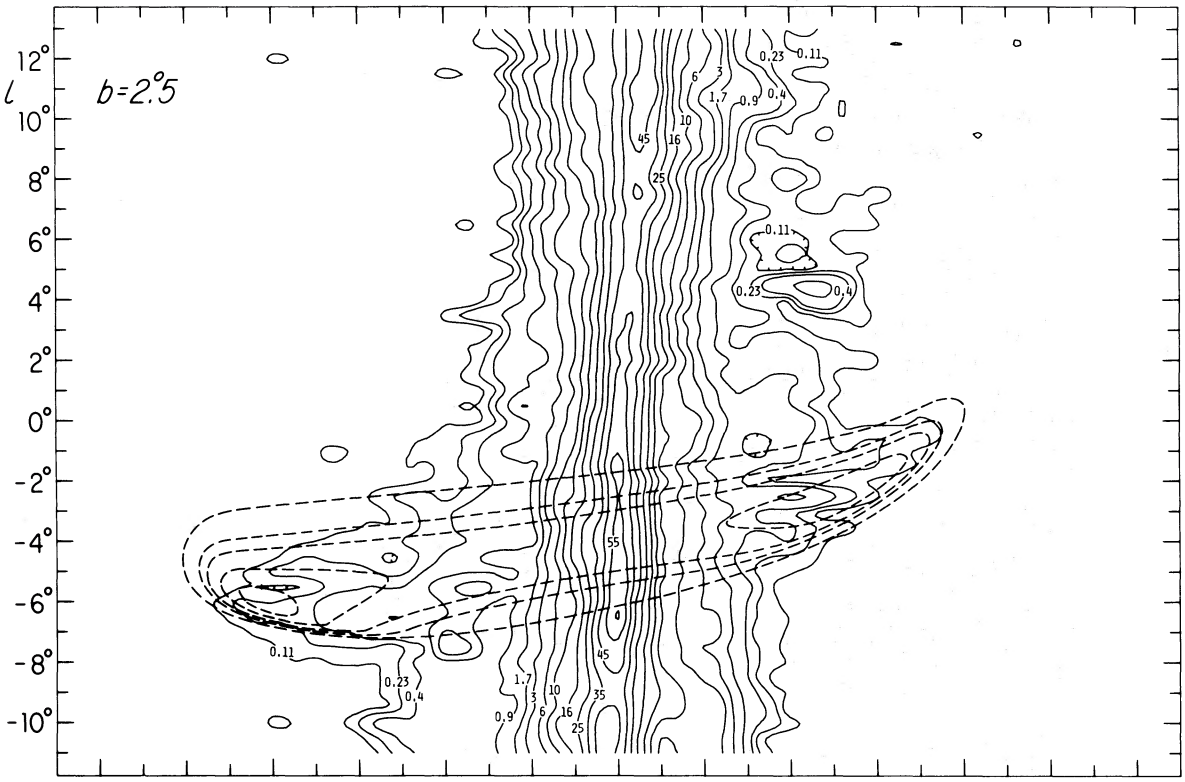

FIG. 6c

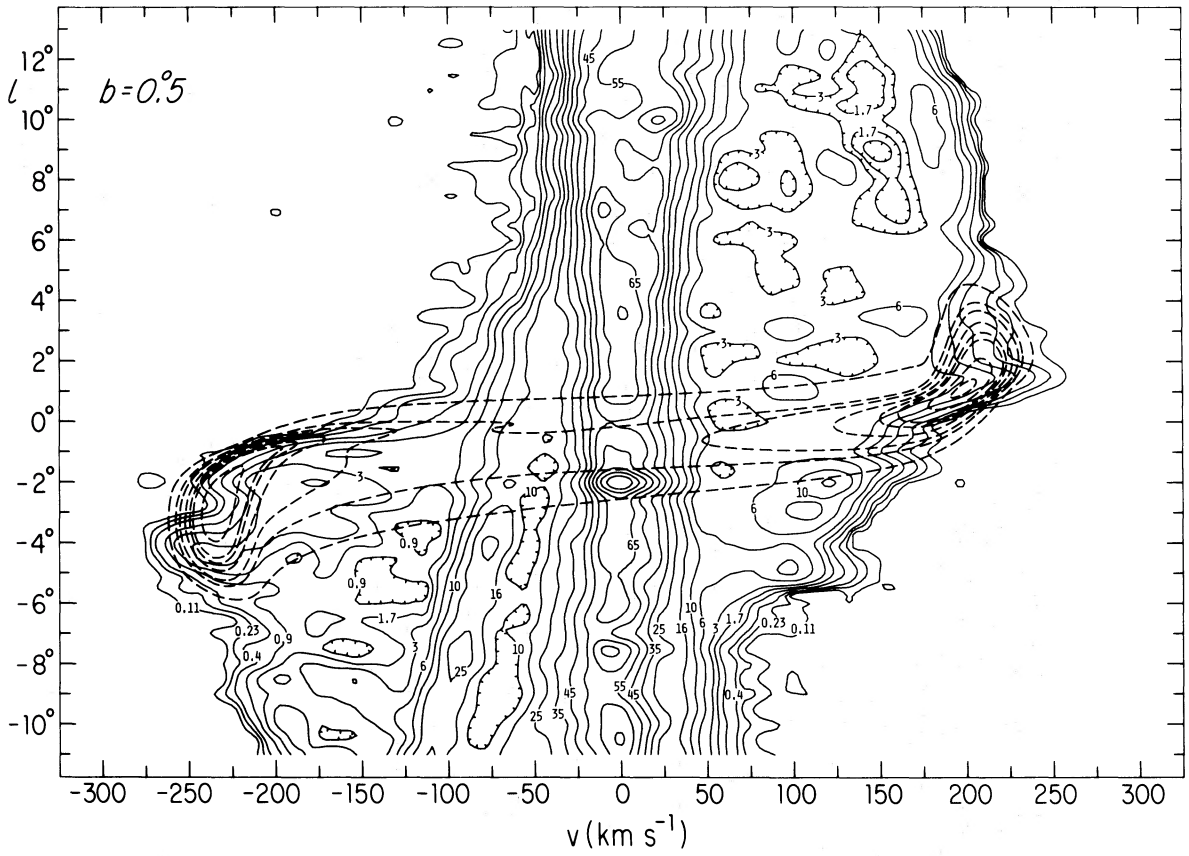

FIG. 6d

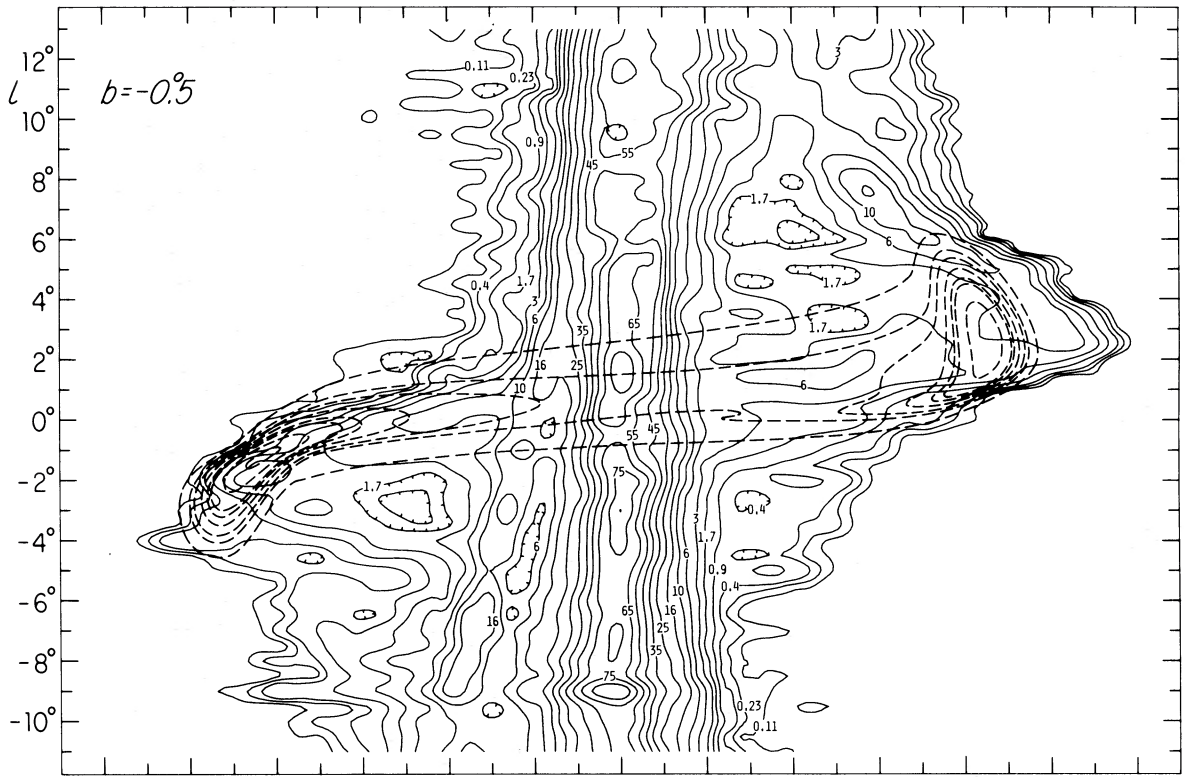

FIG. 6e

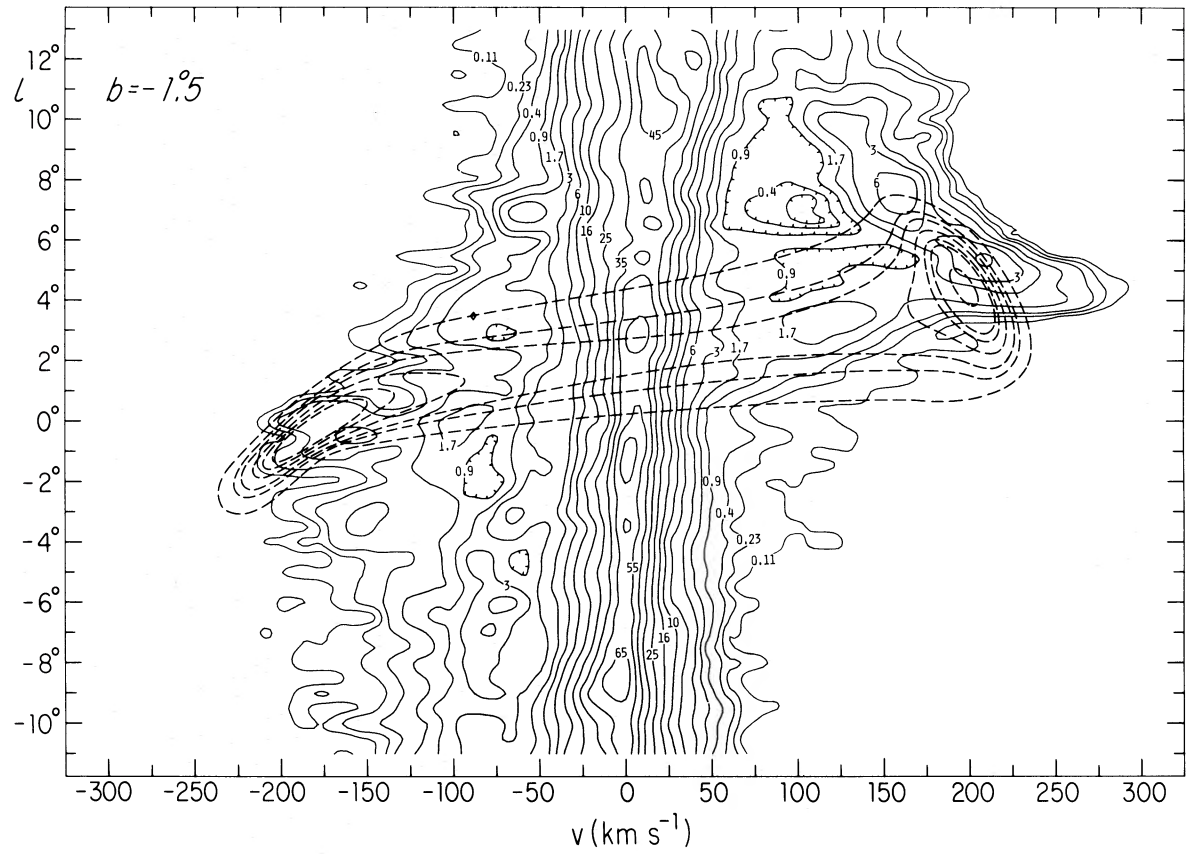

FIG. 6f

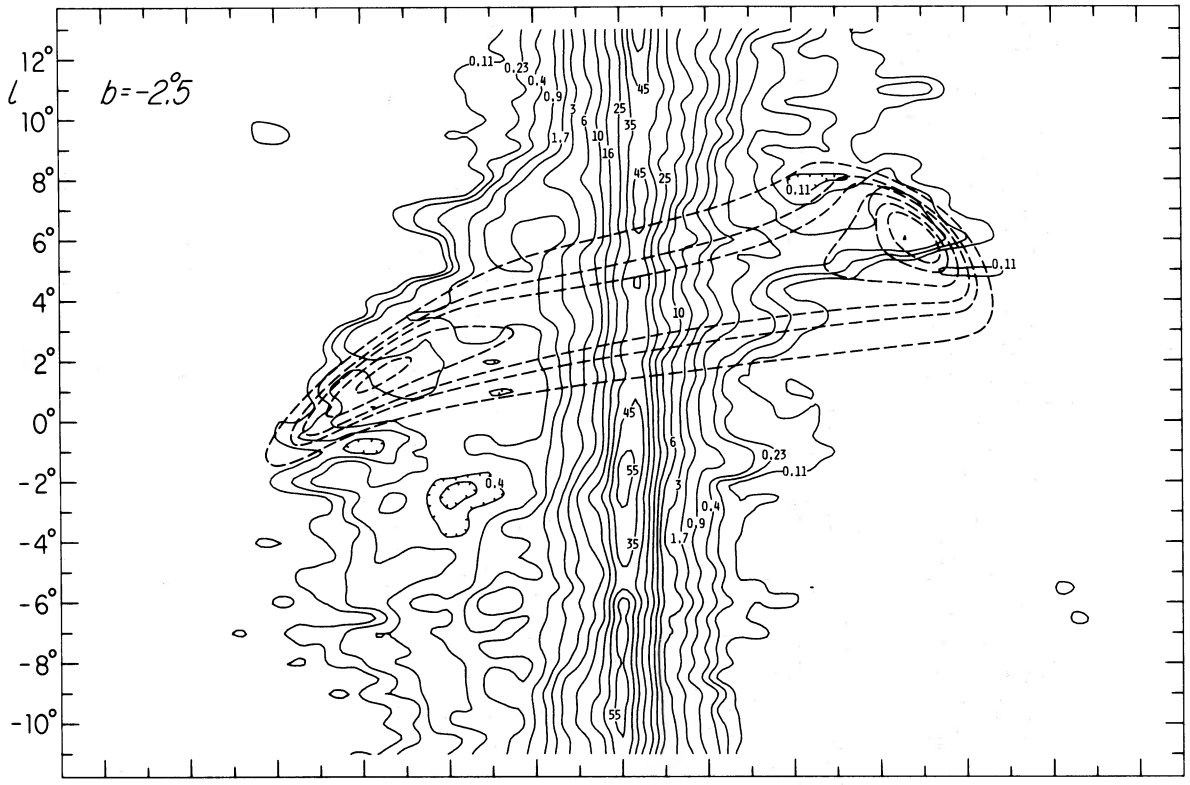

FIG. 6g

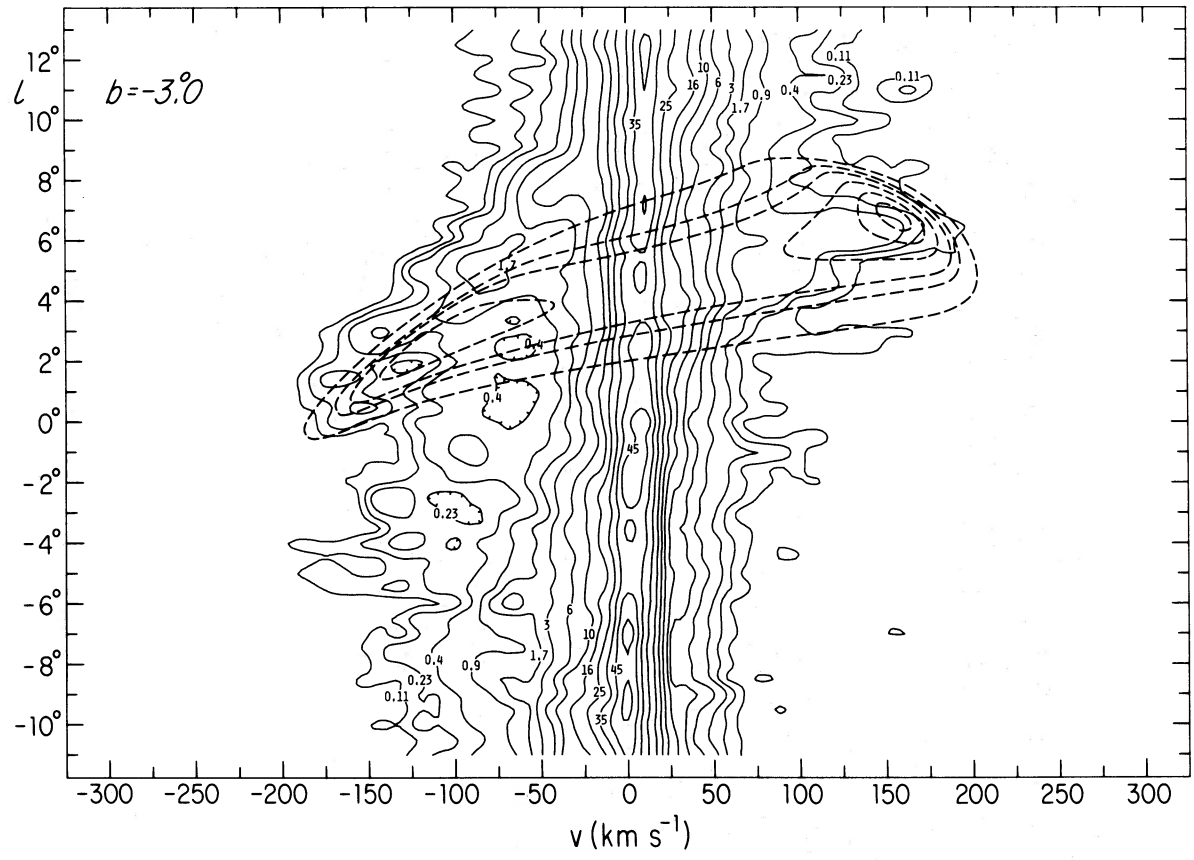

FIG. 6h

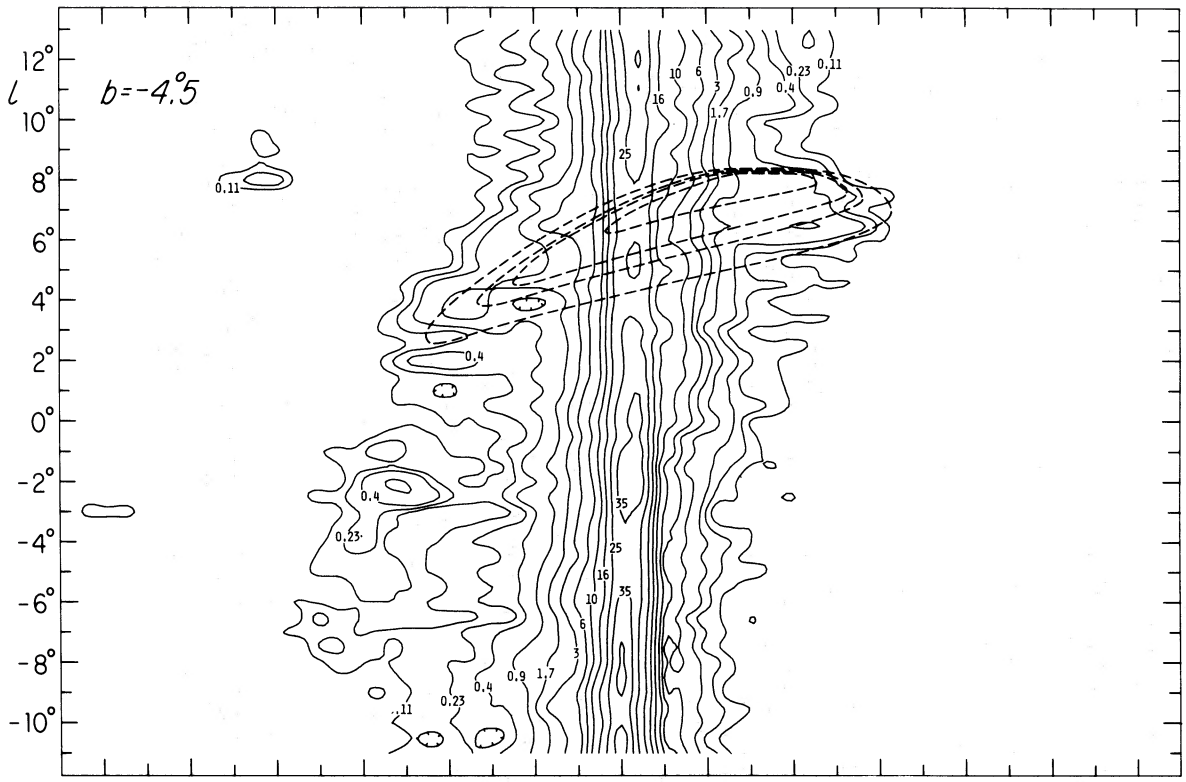

FIG. 6*i*

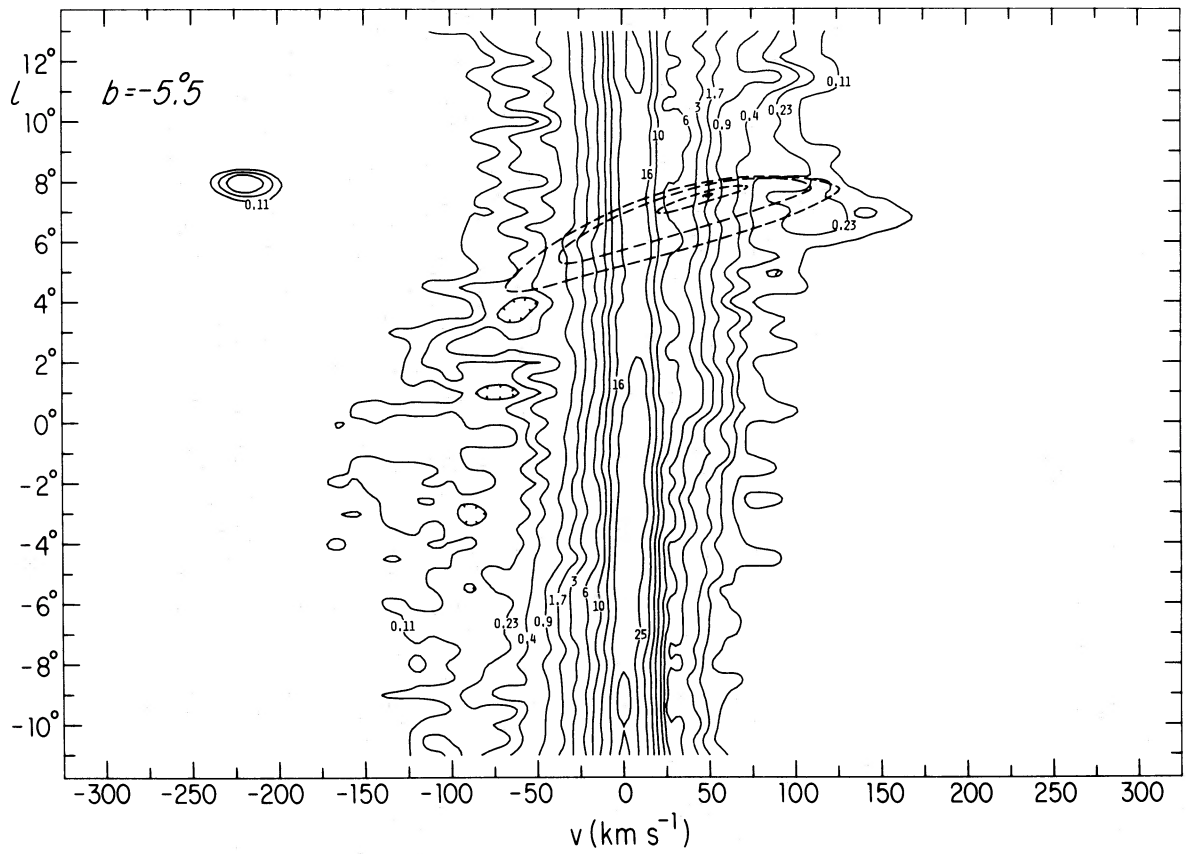

FIG. 6*j*

viii) $b = -5\overset{\circ}{.}5$ (Fig. 6*j*).—This figure should be compared with the corresponding diagram at $b = +4\overset{\circ}{.}5$. The disk signature is more pronounced in the lower-latitude observations because they sample portions of the gas distribution which are substantially nearer to the Sun. The disk signature does not disappear in the observations until $b = 6\overset{\circ}{.}0$, where the predicted pattern is very weak. Comparison of the most extreme (l, v)-diagrams in the current work with those of Paper I at $b = +4\overset{\circ}{.}5$ indicates that the elliptical disk is better able than the circular disk to reproduce the observations. Projection effects are more pronounced in the current model, and are more readily visible in the newer data as well.

b) The Molecular Data

For the sake of completeness, we show in Figure 7 the elliptical disk signature expected of an optically thick gas observed around Sgr A. This diagram was prepared with model gas parameters identical to those used to produce Figure 3 of Paper II; it may be compared with the situation in the 2.6 mm spectral line of CO shown in Figure 2 of Paper II. Two "expanding" features are present which have the spatial extent observed for the proposed "molecular ring" and "165 km s^{-1} expanding feature." As with the circular model, the synthetic profiles do not straightforwardly reproduce the small velocity asymmetry between the two observed emission components, which may be due to a small displacement of the center of the model from the exact position of Sgr A (West) (see Paper II), or to the slight offset of all emission toward the galactic center as discussed in § IV*b*.

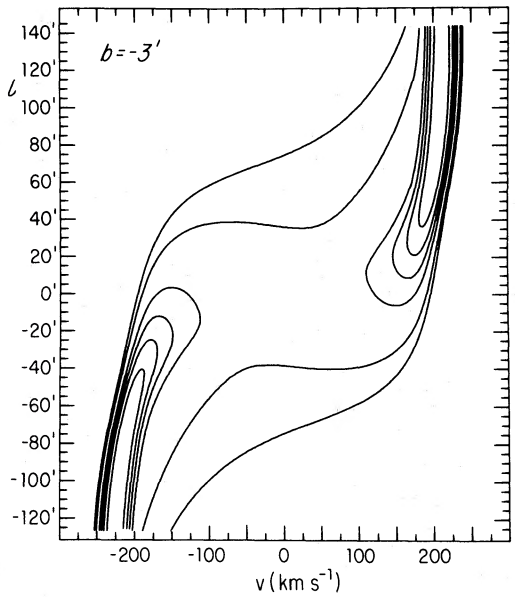

FIG. 7.—A model-generated (l, v)-diagram representing emission at the latitude of Sgr A from an optically thick gas of low excitation temperature (^{12}CO) confined to the tilted elliptical disk. This figure was generated using $n_{CO} = 7 \times 10^{-3}$ cm^{-3}, $T_{exc} = 9$ K, and contains contours drawn at levels $T_A = 0.6, 1.0, 2.0, \ldots, 5.0$ K. This diagram can be compared with the observed molecular distribution shown in Fig. 2 of Paper II and with the results of the circular disk model discussed there.

VI. SUMMARY OF THE RESULTS OF MODELING THE INNER-GALAXY GAS DISTRIBUTION IN TERMS OF A TILTED ELLIPTICAL DISK

1. The tilted elliptical disk model described here provides reproduction of a wide variety of behavior observed in the galactic core region in both H I and CO tracers. The spectral features reproduced by data simulated according to the terms of the model include features with obviously noncircular motions, features with "permitted" kinematics, and features lying both near and away from the galactic equator.

2. The tilted elliptical disk model involves motions along closed streamlines. Although it shares with the tilted circular disk model of Papers I and II the ability to account for most of the apparently isolated spectral features without invoking the existence of separate material concentrations or separate kinematic perturbations, it has the advantage over the earlier model that no net flux of gas out of the galactic center is required.

3. The motivation for the tilted elliptical disk model can find some additional basis both in observation and in theory. Thus de Vaucouleurs and Freeman (1972) have estimated that as many as half of all spiral systems possess a central bar; current theories (e.g., Sanders 1979; Roberts 1979) also emphasize the natural role which bars can play in the dynamics of galaxies. To the extent that the tilted elliptical disk model satisfies the data and to the extent that it represents a dynamically plausible (albeit simplified) situation, it seems not unreasonable to consider that we live in a barred spiral galaxy.

In this series of papers, we have employed kinematic modeling as a means of demonstrating a direct connection between the bulk properties of the inner-Galaxy gas distribution and the appearance there of a multitude of discrete spectral features. The work to date has consisted of a simultaneous exposition of the observations requiring a tilted geometry and pervasive field of noncircular velocities and an interpretation, in great detail, using simple models incorporating these properties. Clearly, the kinematic modeling process cannot provide a unique phenomenological description, nor does it provide direct information on the inner-Galaxy dynamics. Rather, a judicious choice of descriptive models may reasonably be expected to constrain dynamical models in such a way as to lead to a more complete synthesis with wider application to galactic structure as a whole. In terms of the present description, we wish to reiterate several points crucial to our interpretation:

1. There is an actual, coherent body or pattern existing with $\sim$2 kpc of the galactic center; the kinematics required to describe this phenomenon have a high degree of internal symmetry even though a wide variety of seemingly disparate kinematic behavior may be observed at the location of the Sun.

2. Any distinction between permitted and forbidden gas velocities is arbitrary and probably misleading. Most of the gas exhibiting high permitted velocities in the galactic center may rather directly be shown to partake of substantial noncircular motions; alternatively, models incorporating ubiquitous noncircular motions can be shown to produce a fair proportion of their emission at purely permitted velocities. Thus, the gravitational field in the inner portions of the Galaxy cannot necessarily be obtained from the assumption that the highest velocity observed in a given direction is an equilibrium circular velocity.

3. To the extent that the smoothly varying and very large-scale properties of the kinematic models subsume nearly all features thought previously to be the result of violent, episodic activity (ejection) in the galactic nucleus, we believe that there is little or no conclusive evidence for such activity in terms of actual discrete gas packets moving outward from the nucleus. Both models presented by us have employed only a steady flow without locally defined density contrasts; only one requires net flow of mass away from the galactic center.

We have profited from several discussions with J. P. Ostriker of Princeton University on the subject of elliptical streamlines and would like to thank R. H. Sanders for a critical reading of the manuscript. We are also happy to acknowledge the help which A. Phillips of the University of Minnesota gave during the latest observing session in Green Bank.

REFERENCES

Braes, L. L. E. 1963, *Bull. Astr. Inst. Netherlands*, **17**, 132.
Burton, W. B. 1971, *Astr. Ap.*, **10**, 76.
Burton, W. B., Gallagher, J. S., and McGrath, M. A. 1977, *Astr. Ap. Suppl.*, **29**, 123.
Burton, W. B., and Liszt, H. S. 1978, *Ap. J.*, **225**, 815 (Paper I).
Cohen, R. J. 1975, *M.N.R.A.S.*, **171**, 659.
———. 1979, in *IAU Symposium 84, The Large Scale Characteristics of the Galaxy*, ed. W. B. Burton (Dordrecht: Reidel), p. 341.
Cohen, R. J., and Davies, R. D. 1976, *M.N.R.A.S.*, **175**, 1.
de Vaucouleurs, G., and Freeman, K. C. 1972, in *Vistas in Astronomy*, ed. A. Beer (Oxford: Pergamon Press), **14**, 163.
Hulsbosch, A. N. M. 1968, *Bull. Astr. Inst. Netherlands*, **20**, 33.
Kaifu, N., Kato, T., and Iguchi, T. 1972, *Nature Phys. Sci.*, **238**, 105.
Kerr, F. J. 1962, *M.N.R.A.S.*, **123**, 327.
———. 1967, in *Radio Astronomy and the Galactic System*, ed. H. van Woerden (London: Academic Press), p. 239.
———. 1969, in *IAU Symposium 38, The Spiral Structure of Our Galaxy*, ed. W. Becker and G. Contopolous (Dordrecht: Reidel), p. 95.
Kerr, F. J., and Sinclair, M. W. 1966, *Nature*, **212**, 166.
Lacy, J. H., Baas, F., Townes, C. H., and Geballe, T. R. 1979, *Ap. J. (Letters)*, **227**, L17.
Liszt, H. S., and Burton, W. B. 1978, *Ap. J.*, **226**, 790 (Paper II).
Oort, J. H. 1968, in *IAU Symposium 29, Nonstable Phenomena in Galaxies*, ed. M. Arakeljan (Yerevan: Armenian Acad. Sci.), p. 41.
Oort, J. H. 1977, *Ann. Rev. Astr. Ap.*, **15**, 295.
Peters, W. L., III. 1975, *Ap. J.*, **195**, 617.
Roberts, W. W. 1979, in *IAU Symposium 84, The Large Scale Characteristics of the Galaxy*, ed. W. B. Burton (Dordrecht: Reidel), p. 175.
Rougoor, G. W. 1964, *Bull. Astr. Inst. Netherlands*, **17**, 381.
Rougoor, G. W., and Oort, J. H. 1960, *Proc. Nat. Acad. Sci. (USA)*, **46**, 1.
Sanders, R. H. 1979, in *IAU Symposium 84, The Large Scale Characteristics of the Galaxy*, ed. W. B. Burton (Dordrecht: Reidel), p. 383.
Sanders, R. H., and Wrixon, G. T. 1972*a*, *Astr. Ap.*, **18**, 92.
———. 1972*b*, *Astr. Ap.*, **18**, 467.
Sanders, R. H., Wrixon, G. T., and Penzias, A. A. 1972, *Astr. Ap.*, **16**, 322.
Saraber, M. J. M., and Shane, W. W. 1974, *Astr. Ap.*, **36**, 365.
Scoville, N. Z. 1972, *Ap. J. (Letters)*, **175**, L127.
Shane, W. W. 1972, *Astr. Ap.*, **16**, 118.
Simonson, S. C., III, and Mader, G. L. 1973, *Astr. Ap.*, **27**, 337.
Sinha, R. 1979*a*, in *IAU Symposium 84, The Large Scale Characteristics of the Galaxy*, ed. W. B. Burton (Dordrecht Reidel), p. 341.
———. 1979*b*, in *IAU Symposium 84, The Large Scale Characteristics of the Galaxy*, ed. W. B. Burton (Dordrecht: Reidel), p. 599.
van der Kruit, P. C. 1970, *Astr. Ap.*, **4**, 462.

W. B. Burton: Department of Astronomy, University of Minnesota, 116 Church Street S.E., Minneapolis, MN 55455

H. S. Liszt: National Radio Astronomy Observatory, Edgemont Road, Charlottesville, VA 22901